Calculation of Liquid Water−Hydrate−Methane Vapor Phase Equilibria from Molecular Simulations

Lars Jensen,[†] Kaj Thomsen,[†] Nicolas von Solms,[†] Scott Wierzchowski,[‡,#] Matthew R. Walsh,[‡] Carolyn A. Koh,[‡] E. Dendy Sloan,[‡] David T. Wu,[‡,§] and Amadeu K. Sum*[,‡]

Center for Energy Resources Engineering, Department of Chemical & Biochemical Engineering, Technical University of Denmark, 2800 Kgs. Lyngby, Denmark, and Center for Hydrate Research, Department of Chemical Engineering, and Department of Chemistry, Colorado School of Mines, Golden, Colorado 80401

Received: November 20, 2009; Revised Manuscript Received: March 25, 2010

Monte Carlo simulation methods for determining fluid- and crystal-phase chemical potentials are used for the first time to calculate liquid water−methane hydrate−methane vapor phase equilibria from knowledge of atomistic interaction potentials alone. The water and methane molecules are modeled using the TIP4P/ice potential and a united-atom Lennard-Jones potential, respectively. The equilibrium calculation method for this system has three components, (i) thermodynamic integration from a supercritical ideal gas to obtain the fluid-phase chemical potentials, (ii) calculation of the chemical potential of the zero-occupancy hydrate system using thermodynamic integration from an Einstein crystal reference state, and (iii) thermodynamic integration to obtain the water and guest molecules' chemical potentials as a function of the hydrate occupancy. The three-phase equilibrium curve is calculated for pressures ranging from 20 to 500 bar and is shown to follow the Clapeyron behavior, in agreement with experiment; coexistence temperatures differ from the latter by 4−16 K in the pressure range studied. The enthalpy of dissociation extracted from the calculated $P-T$ curve is within 2% of the experimental value at corresponding conditions. While computationally intensive, simulations such as these are essential to map the thermodynamically stable conditions for hydrate systems.

Introduction

Clathrate hydrates, often called gas hydrates, are ice-like inclusion compounds that generally form at low temperatures and high pressures with guest molecules trapped (enclathrated) inside of hydrogen-bonded water cages. Hydrates are relevant in a variety of scientific and industrial contexts, including climate-change modeling, carbon dioxide sequestration, hydrocarbon extraction, hydrogen and natural gas storage, separation and refrigeration technologies, marine biology, and planetary surface chemistry.[1]

The prediction of hydrate-phase boundaries as a function of temperature, pressure, and composition for various hydrate-forming mixtures, including simple and mixed gas systems, is often performed using the established semiempirical statistical mechanical theory of van der Waals and Platteeuw (vdWP),[1−3] which is an exemplar of the common industrial use of statistical mechanics.[1] However, it is also possible to compute hydrate thermodynamics using molecular simulations with model intermolecular potentials. Such simulation studies can independently evaluate the vdWP approach and may contribute to improving this model. For example, a recent study compared guest occupancies of the vdWP model to Monte Carlo (MC) simulation using the SPC/E water model in combination with a Lennard-Jones 12−6 potential for methane.[4] The comparison suggested that the physical significance of the vdWP approach may be improved by including long-range water−methane interactions while still neglecting guest−guest interactions. This ground-breaking study introduced methods to calculate free energies and chemical potentials in the hydrate phase but did not examine phase boundaries. An earlier study by the same authors did estimate the phase diagram of hydrates but used approximate theories for the fluid-phase calculations.[5] It would therefore be valuable to have an independent determination of the hydrate-phase boundary based only on knowledge of the intermolecular potentials. The present paper reports the first such study to do so.

The study of gas hydrates using molecular simulation is also appealing because it enables the molecular-level analysis of dynamic phenomena such as hydrate formation and dissociation, providing a level of detail unavailable in typical laboratory investigations. For example, it has recently been shown that molecular dynamics (MD) simulation can be utilized to observe the spontaneous nucleation and growth of methane hydrate starting from a phase-separated water and methane system at elevated pressure and low temperature.[6] The potential models used in those simulations were the TIP4P/ice model for water[7] and the united-atom Lennard-Jones model for methane.[8] Considering that the chosen water model was parametrized based on a fit to the ice−water phase diagram, it is encouraging that MD simulations employing the model lead to the formation of a clathrate structure upon cooling and pressurization in the presence of methane.

Calculating the three-phase equilibrium of a gas hydrate system with molecular models and simulations not only provides useful information for comparison and evaluation of established models but also helps define the thermodynamic state of a system when considering simulations of equilibrium and dynamic phenomena, such as nucleation and growth, in which the temperature and pressure are usually specified. From

* To whom correspondence should be addressed. Tel. +1(303) 273-3873. Fax +1(303) 273-3730. E-mail: asum@mines.edu.
[†] Technical University of Denmark.
[‡] Department of Chemical Engineering, Colorado School of Mines.
[§] Department of Chemistry, Colorado School of Mines.
[#] Current address: Shell Global Solutions, Westhollow Technology Center, 3333 Highway 6 South, Houston, TX 77082.

10.1021/jp911032q
Published on Web 04/14/2010

experiments, it is well-known that the driving force for the formation of gas hydrates is strongly dependent on the degree of subcooling or overpressurization relative to the equilibrium hydrate formation temperature or pressure.[9−15] Therefore, it is evident that the driving force, in terms of subcooling/overpressurization, must also be well-defined when considering the formation of gas hydrates in molecular simulations. Nonetheless, all such simulation studies to date have arbitrarily set a temperature and pressure, in the absence of knowledge about the actual hydrate phase boundary, and thus the degree of subcooling or overpressurization for the specific molecular models used.

With these considerations in mind, we have established a procedure to calculate the three-phase equilibrium for the liquid water−hydrate−methane vapor (L_W−H−V) system from molecular simulations. We used different MC simulation methodologies to calculate the chemical potentials of liquid water and methane vapor and the chemical potentials of methane and water in the hydrate phase, from which three-phase equilibrium is determined.

Methods and Models

For a two-component (water and methane), three-phase (L_W−H−V) equilibrium, the chemical potentials (μ) of both species in all phases are equal at a given temperature and pressure, that is

$$\begin{aligned} \mu_W^{L_w} &= \mu_W^H = \mu_W^V \\ \mu_M^{L_w} &= \mu_M^H = \mu_M^V \end{aligned} \tag{1}$$

where the subscripts W and M refer to water and methane, respectively. At equilibrium conditions, dense ordered (hydrate), dense disordered (liquid), and low-density (vapor) phases coexist; thus, thermodynamic integration along multiple paths is required to obtain all of the necessary chemical potentials. For each phase at a specified temperature and pressure, the chemical potential of each species varies with the composition in that phase. This is illustrated for the solid hydrate phase in Figure 1, which plots the methane and water chemical potentials versus the number of methane molecules at a fixed temperature, pressure, and number of water molecules. Similar plots exist for the liquid and vapor phases. For a given temperature and pressure, equality of chemical potentials between two phases for each species, that is, two-phase equilibrium, will occur only at a specific composition in each phase. In accordance with the Gibbs phase rule, three-phase equilibrium can then only occur at the coexistence temperature at a given pressure (or coexistence pressure at a given temperature). At three-phase coexistence conditions, the composition in the hydrate phase to be in equilibrium with the gas phase will be the same as the hydrate composition to be in equilibrium with the liquid phase.

Considerable simplification can be made, however, when a phase at coexistence is nearly pure, as is the case for the nearly pure liquid water and nearly pure methane vapor phases. In these cases, the chemical potential of the majority species ($\mu_W^{L_w}$ or μ_M^V) is well-approximated by its pure-phase chemical potential ($\mu_W^{L_w,0}$ or $\mu_M^{V,0}$). The accuracy of this approximation can be assessed by mixture vapor−liquid equilibrium (VLE) simulations and is found to be extremely good for the system studied here, as detailed below. In the present case, this implies that for a given pressure, the coexistence temperature can be determined as that temperature for which the hydrate composition that satisfies $\mu_W^{L_w} \approx \mu_W^{L_w,0} = \mu_W^H$ is the same hydrate composition that satisfies $\mu_M^H = \mu_M^V \approx \mu_M^{V,0}$.

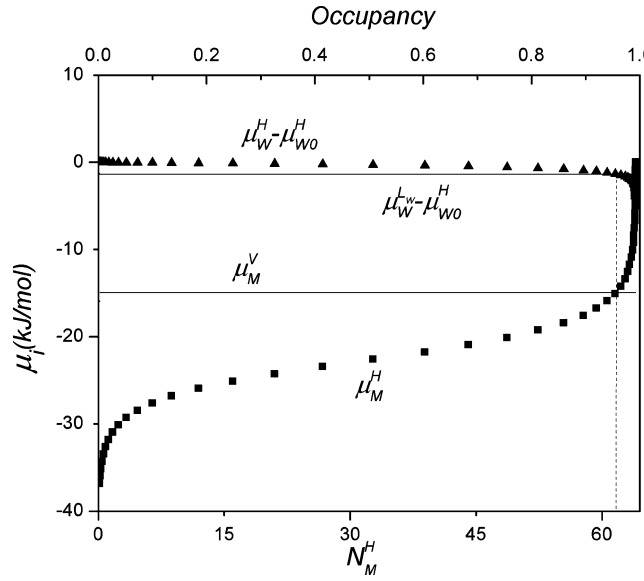

Figure 1. Chemical potential of methane in the vapor phase, μ_M^V (bottom solid line), methane in the hydrate, μ_M^H (squares), water in the liquid phase, $\mu_W^{L_w} - \mu_{W0}^H$ (top solid line), and water in the hydrate phase, $\mu_W^H - \mu_{W0}^H$ (triangles), plotted as a function of the hydrate occupancy. A thermal wavelength, $\Lambda = 1$ Å, was used in calculating the chemical potential for all phases. The number of methane molecules, N_M^H, in the hydrate has a maximum value of 64, corresponding to a $2 \times 2 \times 2$ sI hydrate unit cell. The temperature and pressure here are on the three-phase coexistence curve (298.9 K and 100 bar), and therefore, the condition of equal chemical potentials is satisfied at the same composition, as shown by the vertical dashed line.

Figure 1 illustrates this condition of equal water and equal methane chemical potentials at a given composition (dashed vertical line) required to locate the three-phase equilibrium for a methane hydrate system. The chemical potentials of water in the liquid phase and of methane in the vapor phase are shown as straight lines in the plot, as these are fluid-phase properties independent of the occupancy of methane in the hydrate. Equating these two pairs of chemical potentials is thus sufficient to determine the coexistence temperature, pressure, and hydrate composition. The remaining two chemical potential conditions, $\mu_W^H = \mu_W^V$ and $\mu_M^H = \mu_M^{L_w}$, serve to determine the (dilute) compositions of the minority species in the fluid phases.

The following simulation methods and calculations were performed to obtain each of the chemical potentials in eq 1, allowing determination of the three-phase coexistence temperatures, pressures, and hydrate compositions (cage occupancies) on the L_w−H−V line. The procedure summarized below for the calculation of chemical potentials in the hydrate phase is detailed elsewhere.[4]

Chemical Potential of Water (μ_W^H) and of Methane (μ_M^H) in the Hydrate. The calculation of chemical potentials in the hydrate phase follows the procedure outlined by Wierzchowski and Monson,[4] which we briefly summarize here. The calculation proceeds first by the generation of a hypothetical empty hydrate and calculation of the chemical potential of water therein, followed by integration of the change in chemical potential of both water and methane due to the introduction of methane at various compositions. The latter is carried out using semigrand MC simulations described below.

An equilibrated empty hydrate lattice and its density are first obtained from a *NPT* simulation. The Helmholtz free energy of this empty hydrate, *A*, is then calculated by *NVT* simulations

(at the density determined above) using the methodology described by Frenkel and Ladd;[16] the Frenkel−Ladd method is implemented with modifications to treat the orientational degrees of freedom and the effect of fixed centers of mass.[17,18] Below, we simply refer to this as the FL method. The method is based on thermodynamic integration of the Helmholtz free energy by taking a reversible path to the system of interest from a classical Einstein crystal for which the Helmholtz free energy can be calculated analytically. Once the Helmholtz free energy for the hydrate is known, the chemical potential of water in the empty hydrate is given by

$$\mu_{W0}^{H} = \frac{A + PV}{N_W^H} \tag{2}$$

where, N_W^H, V, and P are the number of water molecules, volume, and pressure of the empty hydrate, respectively.

Methane is then introduced into the hydrate lattice at fixed values of methane chemical potential using N_WPT semigrand MC simulations. For each value of the chemical potential, the number of methane molecules in the hydrate, N_M^H, can be calculated (squares in Figure 1).

The Gibbs−Duhem relation for a two-component system implies that the change in the water chemical potential depends on the change in the methane chemical potential, namely, that at constant temperature and pressure, $N_W^H d\mu_W^H + N_M^H d\mu_M^H = 0$. The water chemical potential in the hydrate can thus be obtained as

$$\mu_W^H - \mu_{W0}^H = -\frac{1}{N_W^H}\int_{-\infty}^{\mu_M^H} N_M^H \, d\mu_M^H \tag{3}$$

and plotted versus N_M^H at the desired temperature and pressure (triangles in Figure 1). From the figure, we can see that the chemical potential of water in the hydrate is less sensitive to the methane occupancy in the hydrate compared to the chemical potential of methane in the hydrate phase. This is understandable as the number of water molecules is much greater than the number of methane molecules.

Finally, note that the Gibbs free energy of the hydrate at any given composition can be expressed as

$$G_H = N_M^H\mu_M^H + N_W^H\mu_W^H = N_M^H\mu_M^H + N_W^H\mu_{W0}^H - \int_{-\infty}^{\mu_M^H} N_M^H \, d\mu_M^H \tag{4}$$

These values can be compared with direct FL thermodynamic integration as a validation of the semigrand method for accounting for hydrate filling, as shown below.

Chemical Potentials of the Fluid Phases ($\mu_{W^w}^L$, μ_W^V, $\mu_{M^w}^L$, μ_M^V). The chemical potentials for a mixture can be expressed as

$$\mu_i(T, P, x_i) = \mu_i^0(T, P) + RT\ln(\gamma_i x_i) \tag{5}$$

where μ_i^0 is the pure component (methane or water) chemical potential at the mixture temperature, T, and pressure, P, x_i is the mole fraction of the pure component, and γ_i is the activity coefficient of species i in the mixture. For nearly pure phases, $x_i \approx 1$ for the majority species, and the Lewis−Randall rule, $\gamma_i = 1 + O(x_i^2) \approx 1$, applies.

The chemical potential of a pure component is found from thermodynamic integration (TI). If the chemical potential at one pressure is known, then the chemical potential at any other pressure along an isotherm can be found as

$$\frac{\mu_i(T, P_2)}{k_BT} = \frac{\mu_i(T, P_1)}{k_BT} + \int_{P_1}^{P_2} \frac{1}{\rho_i k_B T} \, dP \tag{6}$$

where, ρ_i is the number density and k_B is the Boltzmann constant. Likewise, along an isobar, the temperature dependence of the chemical potential is given as

$$\frac{\mu_i(T_2, P)}{k_BT_2} = \frac{\mu_i(T_1, P)}{k_BT_1} - \int_{T_1}^{T_2} \frac{H_i}{k_BT^2} \, dT \tag{7}$$

where H_i is the molar enthalpy of water or methane. The starting point of the thermodynamic integration can be chosen arbitrarily; however, the ideal gas is often a convenient choice given that its chemical potential can be calculated analytically. The ideal gas chemical potential is given by

$$\frac{\mu_i^{id}}{k_BT} = \ln(\rho_i\Lambda^3) \tag{8}$$

where $\Lambda = h/(2\pi m k_B T)^{1/2}$ is the thermal wavelength, with h as Planck's constant and m as the molecular mass; this term cancels out when comparing chemical potentials between phases in equilibrium. From NPT simulations along the thermodynamic integration path, the chemical potential of each fluid is calculated in the temperature and pressure regions of interest.

For testing the assumption that the chemical potentials of the pure phases are good approximations to the chemical potentials of the phases with dissolved methane or water, the fluid solubilities were calculated. The mole fraction of a compound in the gas phase (y_i) for near-ideal conditions can be described well in terms of the partial pressure of the compound

$$y_i = \frac{P_i}{P} \tag{9}$$

where the total pressure, P, is the sum of the partial pressures. Likewise, the solubility of a small nonpolar molecule in an aqueous phase (x_i) is well-described by Henry's law, which is given by

$$k_{H,i} = \frac{P_i}{x_i}y_i \tag{10}$$

Henry's constant can also be related to the excess chemical potential of the solute, $\mu_i^{ex,\infty}$, by

$$k_{H,i} = \rho_s k_B T \exp(\mu_i^{ex,\infty}/k_BT) \tag{11}$$

where ρ_s is the solvent density. The excess chemical potential of the solute can be calculated from test particle insertion (TPI) simulations.[19] The change in chemical potential resulting from the solubility calculations at various T and P conditions can

then be compared in magnitude relative to the pure phase approximations, as shown below.

Simulation Details and Potential Models

The united-atom Lennard-Jones representation using the optimized parameters (OPLS) by Jorgensen was used to model methane.[8] The water molecules were modeled using the TIP4P/ice potential.[7] The cross interactions between methane and water were accounted for with the Lorentz−Berthelot combining rule.[20,21] The TIP4P/ice potential model accurately describes the solid−liquid equilibrium between hexagonal ice and liquid water up to 2000 bar.[7] Considering that hydrate is also a solid with a crystal structure mainly composed of water molecules, it is plausible that the TIP4P/ice model, together with a suitable model for the gas molecules, is capable of describing the thermodynamic properties of gas hydrates.

Monte Carlo simulations used the standard Ewald summation method for the long-range electrostatic forces.[22,23] Similarly, an Ewald summation approach was applied to evaluate the long-range dispersion interactions using a lattice sum method.[24] A convergence parameter of $4/L$ was used, where L is the lattice parameter for sI hydrate. For all simulations, the cutoff radius was 10 Å.

For the fluid phase-simulations, 500 water or methane molecules were used. The enthalpy and density of the fluid phases were obtained from *NPT* simulations. Typically 50 000−100 000 equilibration cycles, followed by 100 000−250 000 production cycles were required to obtain statistically acceptable averages of the densities and enthalpies. A cycle corresponded to a set of N trial moves, where N is the number of molecules in the system. The starting point for the integration path was in both cases 1 bar and 800 K, and the ending points of the integration were between 20 and 500 bar and 270 and 320 K. By performing the *NPT* simulations in small steps of temperature and pressure, the chemical potential for water or methane was obtained from eq 6 or 7 by integration using the trapezoidal rule. Step lengths may vary depending on in which region of the $P-T$ diagram the step is done; however, smooth curves must be used in order to get accurate integration. The solubility of methane in water was found from TPI simulations. Using the methodology described by Bennett,[25] TPI simulations were performed in the *NPT* ensemble to obtain the solvent (water) densities and solute (methane) excess chemical potentials, from which Henry's constants were obtained. The Bennett method was used as it has been reported to offer improved accuracy over the Widom method.[26,27] For these simulations, 500 water molecules were first equilibrated for more than 100 000 cycles, after which four stages of more than 500 000 cycles were performed. In the first stage, insertions of test particles were performed with five insertions attempted per cycle, and in the following three stages, the particles were deleted.

The zero-occupancy empty hydrate lattice consisted of 368 water molecules ($2 \times 2 \times 2$ sI hydrate unit cells); *NPT* simulations were performed for 20 000 equilibration cycles and 200 000 cycles for averaging. The densities obtained were used as input to the semigrand MC and FL simulations. The semigrand MC simulations were conducted over a range of methane chemical potentials (μ_M^H) from states in the neighborhood of the zero-occupancy hydrate (we used an initial value of $\mu_M^H = -36.83$ kJ/mol, which resulted in an occupancy very close to zero) up to states describing a fully occupied hydrate (single occupancy of cages). Integration of eq 3 was done using the trapezoidal rule in intervals of $\delta\mu_M = 0.837$ kJ/mol.

The third simulation type involved the calculation of the chemical potential of water in the zero-occupancy hydrate (μ_{W0}^H), which, according to eq 3, is necessary for calculating the chemical potential of water in the occupied hydrate (μ_W^H). In addition, μ_{W0}^H is used for calculating the Gibbs free energy of the hydrate at any given composition according to eq 4. The Helmholtz free energies of the empty and full hydrate were found using the FL method. The coordinates of the oxygen atoms for the perfect crystal used in specifying the Hamiltonian, $H_E(\lambda_T,\lambda_R)$ were those given for the sI hydrate.[28] The force constants used in the FL method were $\lambda_T = 25000k_BT/Å^2$ and $\lambda_R = 25000k_BT$. Simulations were performed for 5000 relaxation cycles and 50 000 averaging cycles. Calculation of the Helmholtz free energy was performed using a 20 point Gaussian quadrature.

TABLE 1: Vapor−Liquid Equilibria for the Binary Water−Methane System at 100 bar and in the Temperature Range of 275−310 K As Found from Experiments and Monte Carlo Simulations[a]

	$k_{H,M}$ (kbar)		x_M		y_W ($\times 10^4$)	
T (K)	sim.	exp.	sim.	exp.	sim.	exp.
275	34 (5)	24	0.0030	0.0042	0.0257	0.7037
280	39 (5)	27	0.0025	0.0037	0.0372	0.9775
290	35 (6)	34	0.0028	0.0029	0.0766	1.8538
300	59 (6)	41	0.0017	0.0025	0.1540	3.4402
310	102 (12)	47	0.0010	0.0021	0.3024	6.2558

[a] The numbers in parentheses for the simulated Henry's constants indicate the standard deviation.

Results and Discussion

We first consider the calculation of the fluid-phase VLE, which was done at 100 bar and in the temperature range of 275−310 K. The solubility of methane in water was found from the TPI simulations. The fraction of water in the vapor phase was estimated using eq 9 and using the vapor pressure data for water modeled using TIP4P/ice as reported by Chialvo et al.[29] as the water partial pressure; the methane partial pressure was determined by the equilibrium condition with the hydrate phase. Since only the water vapor pressures of TIP4P/ice in the temperature range of 300−650 K were reported, we extrapolated the data to 275 K. Since the vapor pressures show a high degree of linearity in the log P versus $1/T$ plane, the error resulting from the extrapolation should be relatively small. Nonideal effects are assumed to be small in the gas phase under the conditions studied, and in any case, the water partial pressure is so low that the effect on the chemical potentials of the majority species is still negligible. The results of the VLE calculations along with experimental values are provided in Table 1. Experimental Henry's constants were calculated using a semiempirical correlation based on a best fit to experimental data in the temperature range of 273.15−633.15 K.[30,31] The experimental fractions of water found in the vapor phase are based on experimentally determined vapor pressures of water.[32]

As seen from Table 1, the TIP4P/ice water model in combination with the OPLS potential model for methane predicts the solubility of methane in water to be around 30−50% lower than the experimental values, while the amount of water in the vapor phase is on the order of 20−25 times lower than the experimental values. The low solubility of methane (modeled with the OPLS and the TraPPE force fields) in water using other versions of the TIP4P water potential has previously been reported, thus providing additional evidence that the results found here seem reasonable and consistent with existing studies.[33,34]

TABLE 2: Pure Component Chemical Potential of Water and the Contribution to the Liquid Water Chemical Potential from Accounting for the Solubility of Methane in Water[a]

T (K)	μ_W^0 (kJ/mol)	$RT \ln(x_W)$ (kJ/mol)
275	−43.887 (0.06)	−0.007 (0.0010)
280	−43.676 (0.06)	−0.006 (0.0008)
290	−43.276 (0.06)	−0.007 (0.0012)
300	−42.895 (0.07)	−0.004 (0.0004)
310	−42.553 (0.07)	−0.003 (0.0003)

[a] All results are for a pressure of 100 bar. The numbers in parentheses are standard deviations.

According to eq 5, the change in the chemical potential of the majority species when accounting for fluid phases mixing is $RT \ln x_i = RT \ln(1 - x_j) \approx -RTx_j$, where $x_j \ll 1$ is the mole fraction of the minority species, as given in Table 1. Since the mixtures are nearly pure, the activity coefficient is extremely close to unity. Therefore, it is obvious from Table 1 that accounting for mixing will have a higher impact on the chemical potential of liquid water, $\mu_W^{L_W}$, than on that of methane vapor, μ_M^V, since the mole fraction of methane in liquid water, as predicted using the potential models, is on the order of 100−1000 times larger than the mole fraction of water in methane vapor. In Table 2, the pure component chemical potential of water, found from TI and the additional excess contribution to the total chemical potential due to the dissolved methane, is shown at 100 bar and in the temperature range of 275−310 K. It is evident that the contribution from mixing to the chemical potential of water is negligible compared to the pure water chemical potential (the mixing contribution to the chemical potential is less than the standard deviation from the combined TI steps that were used to calculate the pure water chemical potential). From these considerations, we conclude that the fluid phases can be considered pure for the purposes of determining the chemical potential as the effects of mixing on the pure component chemicals potentials are negligible and consequently have no significant influence when calculating the three-phase (L_W−H−V) equilibrium.

Next, we consider the calculation of the Gibbs free energies of the zero-occupancy and fully occupied hydrates directly using the FL method. The results obtained using semigrand MC simulations, together with eq 4, can also yield the Gibbs free energy of a fully occupied hydrate. Typical results obtained for the semigrand MC simulations correspond to the squares in Figure 1, which shows the methane occupancy of the hydrate as a function of the chemical potential for methane in the hydrate. As seen in the figure, the chemical potential of methane increases as the hydrate is filled with methane. At a chemical potential of about −10 kJ/mol, the number of methane molecules asymptotically approaches full occupancy of the hydrate (64 for the 2 × 2 × 2 unit cells of sI hydrate considered).

Table 3 shows the results of a thermodynamic consistency test. Here, we compare the Gibbs free energy of the fully occupied hydrate found from thermodynamic integration from the zero-occupancy hydrate (using eq 4) with the free energy of an occupied hydrate calculated directly using the FL method. The table shows the results obtained at 100 bar and in the temperature interval of 285−300 K. There is good agreement between the two methods, indicating that these two independent methods for estimating the chemical potential of methane in the hydrate are consistent. These results are also in good agreement with a previous study.[4]

To obtain the three-phase equilibrium temperature at a given pressure, it is necessary to satisfy the constraint on the equality

TABLE 3: Gibbs Free Energy of Water of a Zero-Occupancy and a Full-Occupancy Hydrate Calculated with the FL Method[a]

T (K)	zero-occupancy hydrate (FL) (kJ/mol)	full hydrate (FL) (kJ/mol)	full hydrate (TI) (kJ/mol)
285	−42.40 (0.11)	−46.26 (0.06)	−46.34 (0.11)
290	−42.09 (0.05)	−45.98 (0.06)	−46.03 (0.05)
295	−41.81 (0.06)	−45.69 (0.07)	−45.75 (0.06)
300	−41.51 (0.06)	−45.40 (0.07)	−45.45 (0.06)

[a] The full hydrate value calculated from a zero-occupancy hydrate reference by thermodynamic integration (TI) is also shown. A thermal wavelength of $\Lambda = 1$ Å was used. Calculations were performed at 100 bar and the specified temperature. Numbers in parentheses are standard deviations.

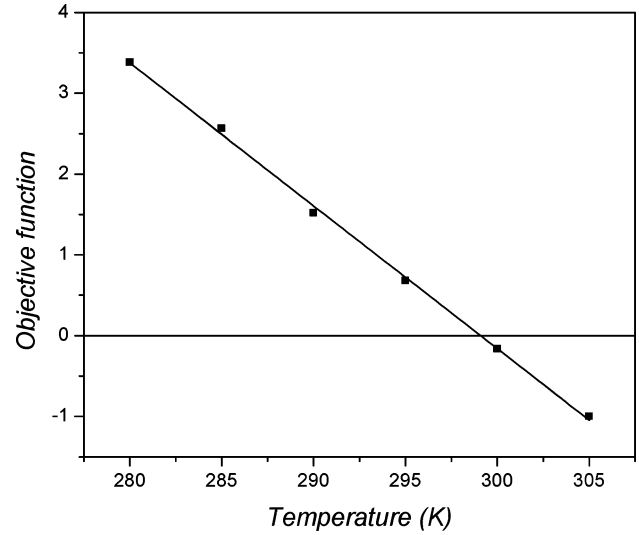

Figure 2. Value of the objective function (OF) defined by eq 12 at the different temperatures explicitly considered at 100 bar (squares). The line corresponds to the best fit of the points. The objective function has an interpolated value of zero (condition for equilibrium) for the liquid water−hydrate−methane vapor equilibrium at 298.9 K.

of the chemical potential for each species in each phase, as shown in eq 1, and with the same hydrate composition as that discussed earlier. Therefore, we employ the following objective function (OF) describing the difference in the methane occupancies at which the chemical potentials of both components are equal

$$\mathrm{OF} = N_M(\mu_M^V = \mu_M^H) - N_M(\mu_W^{L_W} = \mu_W^H) \qquad (12)$$

Conditions for equilibrium are met when the OF has a value of 0. In practice, the OF is calculated at constant pressure for different temperatures, spanning a certain region within the expected equilibrium temperature. Figure 2 shows the values of the OF for the temperatures explicitly considered in the simulations at the fixed pressure of 100 bar. The OF exhibits a high degree of linearity with temperature in the range examined, thus allowing interpolation to obtain the coexistence temperature. The same procedure was applied to determine the equilibrium temperature at the other pressures.

On the basis of this procedure, the calculated three-phase equilibrium temperatures for liquid water−methane hydrate−methane vapor in the pressure range of 20−500 bar are shown in Figure 3 along with experimental data. It can be seen that the linear behavior exhibited by the experimental data is also

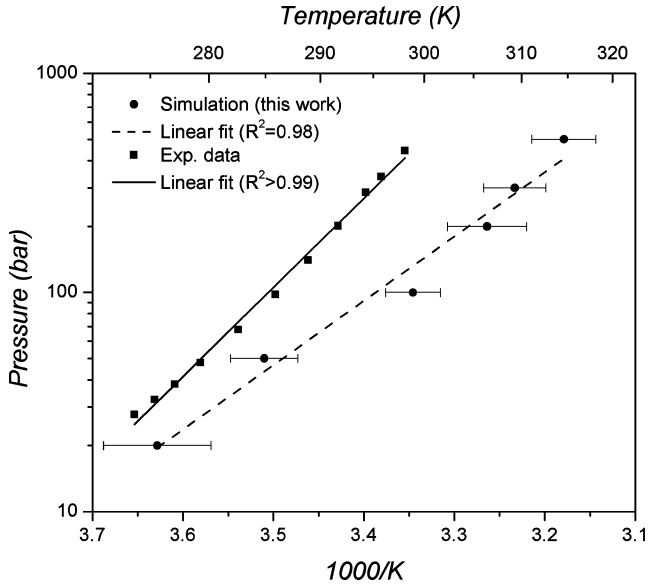

Figure 3. Pressure−temperature phase diagram for the liquid water−methane hydrate−methane vapor system comparing experimental data (squares)[35−37] and MC simulations results (circles). The straight lines correspond to the best fit of the data as found from a data regression. The error bars on the points found from simulation correspond to uncertainty in the temperature estimated from the standard deviations of μ_M^H, μ_M^V, $(\mu_W^{L_W} - \mu_{W0}^H)$, and $(\mu_W^H - \mu_{W0}^H)$.

seen in the simulation data; it has been shown in general that coexistence curves of simple hydrates approximate straight lines in log P versus $1/T$ plots. The Clapeyron equation applied to simple hydrates relates the equilibrium pressures and temperatures to the dissociation enthalpy[38]

$$\frac{\mathrm{d}\log P}{\mathrm{d}(1/T)} = -\frac{\Delta H}{zR} \tag{13}$$

where ΔH is the dissociation enthalpy of the hydrate, z is the compressibility factor of the gas, and R is the universal gas constant. The experimental value for the enthalpy of dissociation has been reported at 273.15 K and 24.98 bar.[39,40] For this reason, the equilibrium data calculated from simulation has been extrapolated to 273.15 K, which corresponds to a pressure of 16.71 bar; the enthalpy of dissociation was calculated at these conditions using eq 13. Similarly, we have found the enthalpy of dissociation from simulation at the experimental pressure of 25 bar, which corresponds to a temperature of 277.95 K (that is, the enthalpy of dissociation was determined at both the reported experimental pressure and temperature, at conditions corresponding to the equilibrium temperature or pressure, respectively, as calculated from simulation). The compressibility factor in eq 13 for methane was determined from methane *NPT* simulations at the corresponding temperature and pressure. The results for the enthalpy of dissociation are shown in Table 4. As can be seen from the results, the enthalpy of dissociation of methane hydrate found from simulations is within 2% of the experimental value at similar conditions. The enthalpy of dissociation found at 277.95 K from the simulations is slightly lower than the one found at 273.15 K, which is due to the compressibility factor of methane being smaller at 25 bar compared to that at 16.71 bar.

Figure 4 shows the fractional (small/large cage) and total equilibrium hydrate occupancy as a function of pressure, as determined from the simulations. As seen in the figure, the

TABLE 4: Enthalpy of Dissociation for Methane Hydrate Determined from the Clapeyron Equation Using Simulation Data for the Three-Phase Equilibrium[a]

	ΔH (kJ/mol CH_4)
from simulation data at 273.15 K and 16.71 bar	53.9
from simulation data at 277.95 K and 25 bar	53.1
from experimental data at 273.15 K and 24.97 bar	54.2

[a] Experimental values obtained from Handa.[39,40]

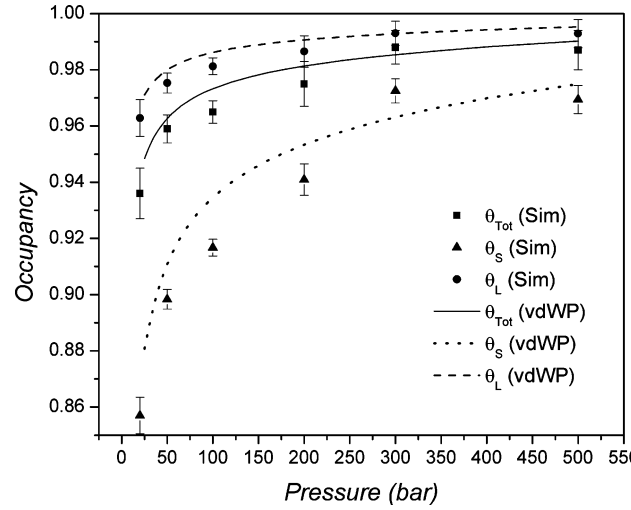

Figure 4. Fractional (small and large cage) and total occupancy of the methane hydrate from MC simulations and calculated from the vdWP approach, which assumes Langmuir adsorption isotherms for methane in the hydrate. The Langmuir constants used to calculate the occupancy are those reported by Munck and co-workers.[41] The error bars in the occupancy correspond to the uncertainty estimated from the standard deviations of μ_M^H, μ_M^V, $(\mu_W^{L_W} - \mu_{W0}^H)$, and $(\mu_W^H - \mu_{W0}^H)$.

occupancy increases as the equilibrium pressure increases. It has previously been shown that the occupancy, $\theta_{J,i}$, of cavity i by type J molecules follows a Langmuir adsorption relation, which is applied in the vdWP theory

$$\theta_{J,i} = \frac{C_{J,i} f_J}{1 + C_{J,i} f_J} \tag{14}$$

where $C_{J,i}$ are the Langmuir constants found from fitting experimental data and f_J are the fugacities of molecule J. Using the Langmuir constants for methane as reported by Munck and co-workers,[41] the fractional and total occupancies of methane hydrate as a function of the equilibrium pressure are also plotted in Figure 4. As seen in the figure, there is good agreement between the trends observed in the occupancy found from simulation and those predicted by the Langmuir adsorption relation applied in the vdWP theory. Similar observations for the methane and propane hydrate occupancy as a function of pressure have been presented in the literature.[42,43]

In general, the occupancies found from simulations are slightly lower compared to those predicted by the vdWP theory. Compared to that of the large cages, the occupancy of the small cages is seen to be more strongly dependent on the pressure, both as calculated from simulation and from the vdWP theory. At the same time, the small cage occupancies found from simulations deviate more from those predicted by the vdWP theory when compared to the relative deviation in the large cage occupancies. The small/large cage occupancy ratios found from

simulations were between 0.89 and 0.98, and the hydration numbers were found to vary between 6.15 and 5.82 in the pressure region investigated; both of these quantities are not only within the limits reported from theoretical studies but are also within the experimentally reported values.[1,44−50]

The small differences in occupancy between those from simulation and those predicted by the vdWP theory may be explained by revisiting some of the underlying assumptions of the vdWP theory. Previous studies have shown that the neglect of long-range interactions between methane−methane and methane−water in the vdWP theory can cause minor changes in the occupancy; additionally, the effect of assuming a static hydrate framework can have a significant effect on the occupancy relationship, particularly for small cage occupancy.[4]

Conclusions

Monte Carlo simulations were used to calculate the three-phase liquid water−methane hydrate−methane vapor equilibrium in the pressure range of 20−500 bar based on molecular models for water (TIP4P/ice) and methane (united-atom Lennard-Jones). Vapor−liquid equilibria calculations for the binary methane−water system showed that the fluid phases were nearly pure for the conditions studied, and thus, the effect of accounting for mixing in these phases had a negligible contribution to the chemical potential of the majority species. For this reason, the pure component values could be used for the chemical potentials of liquid water and methane vapor to simplify the criteria for phase coexistence. In general, good agreement between the simulated and experimental three-phase coexistence curves was found. The deviation in the coexistence temperature between the simulation and experimental data increased with pressure, from 4 K at 20 bar to 16 K at 500 bar. The calculated three-phase equilibrium curve was closely fit by a straight line on a log P versus $1/T$ plot, indicating that the data follow a Clapeyron equation relation, a behavior also seen in the experimental data. An enthalpy of hydrate dissociation of about 53 kJ/mol was obtained at 273.15 K or 25 bar, which is within 2% of the experimental value of 54.2 kJ/mol at these conditions. The hydrate occupancies found at equilibrium from the simulations are in reasonably good agreement with those calculated from the van der Waals and Platteeuw approach, which uses a Langmuir adsorption analogy. The results obtained from this study are the first to determine the phase diagram of a gas hydrate system using only the results of atomistic molecular simulations and analytical calculations.

Determining the phase equilibrium of a multicomponent, multiphase system is an intricate and computationally intensive process; however, such calculations are essential if proper conclusions are to be made from hydrate simulations defined in terms of subcooling or overpressurization. The methodology and results reported here serve as a foundation for future studies investigating both equilibrium and dynamic simulations employing molecular models. It should be noted that the presented results are specific to the molecular models used, and phase boundaries may differ significantly between different molecular models; caution should be exercised when determining whether a simulated system is thermodynamically stable within the hydrate phase envelope.

Acknowledgment. The authors would like to thank the Danish Research Council for Technology and Production Sciences for financial support through the project "Gas Hydrates-from Threat to Opportunity" and the Technical University of Denmark for financial support through a Ph.D. scholarship. This research was supported in part by the Golden Energy Computing Organization at the Colorado School of Mines using resources acquired with financial assistance from the National Science Foundation and the National Renewable Energy Laboratory. A.K.S. and D.T.W. acknowledge the support from the National Science Foundation under Grant CBET-0933856. We acknowledge the financial support from the Center for Hydrate Research Consortium at the Colorado School of Mines (BP, Champion, Chevron, ConocoPhilips, ExxonMobil, Haliburton, Multichem, Nalco, Petrobras, Schlumberger, Shell, StatoilHydro, and Total). A.K.S. acknowledges the support of DuPont for a DuPont Young Professor Award. M.R.W. was supported by funds from U.S. Department of Energy, Basic Energy Sciences (DOE-BES) under Contract DE-FG02-05ER46242.

Note Added after ASAP Publication. This article posted on April 14, 2010. The last sentence in the Acknowledgment section has been added. The correct version posted on April 29, 2010.

References and Notes

(1) Sloan, E. D., Koh, C. A., *Clathrate Hydrates of Natural Gases*, 3rd ed.; CRC Press: Boca Raton, FL, 2008.
(2) van der Waals, J. H. *Trans. Faraday Soc.* **1956**, *52*, 184.
(3) van der Waals, J. H.; Platteeuw, J. C. *Adv. Chem. Phys.* **1959**, *2*, 1.
(4) Wierzchowski, S. J.; Monson, P. A. *J. Phys. Chem. B* **2007**, *111*, 7274.
(5) Wierzchowski, S. J.; Monson, P. A. *Ind. Eng. Chem. Res.* **2006**, *45*, 424.
(6) Walsh, M. R.; Koh, C. A.; Sloan, E. D.; Sum, A. K.; Wu, D. T. *Science* **2009**, *326*, 1095.
(7) Abascal, J. L. F.; Sanz, E.; Garcia, R.; Vega, C. *J. Chem. Phys.* **2005**, *122*, 234511.
(8) Jorgensen, W. L.; Madura, J. D.; Swenson, C. J. *J. Am. Chem. Soc.* **1984**, *106*, 6638.
(9) Vysniauskas, A.; Bishnoi, P. R. *Chem. Eng. Sci.* **1983**, *38*, 1061.
(10) Skovborg, P.; Rasmussen, P. *Chem. Eng. Sci.* **1994**, *49*, 1131.
(11) Natarajan, V.; Bishnoi, P. R.; Kalogerakis, N. *Chem. Eng. Sci.* **1994**, *49*, 2075.
(12) Christiansen, R. L., Sloan, E. D., *Proceedings of the Annual Convention of Gas Processors Association*; San Antonio, TX, 1995; Vol. 74, p 15.
(13) Kashchiev, D; Firoozabadi, A. *J. Cryst. Growth* **2002**, *243*, 476.
(14) Anklam, A. F.; Firoozabadi, A. *J. Chem. Phys.* **1999**, *103*, 3977.
(15) Armandi, M.; Tohidi, B.; Danesh, A.; Todd, A. C. *Chem. Eng. Sci.* **2005**, *60*, 1313.
(16) Frenkel, D.; Ladd, A. D. C. *J. Chem. Phys.* **1984**, *81*, 3188.
(17) Vega, C.; Monson, P. A. *J. Chem. Phys.* **1998**, *109*, 9938.
(18) Polson, J. M.; Trizac, E.; Pronk, S.; Frenkel, D. *J. Chem. Phys.* **2000**, *112*, 5339.
(19) Widom, B. *J. Chem. Phys.* **1963**, *39*, 2802.
(20) Lorentz, H. A. *Ann. Physik* **1881**, *12*, 127.
(21) Berthelot, D. *C.R. Acad. Sci. Paris* **1889**, *126*, 1703.
(22) Heyes, D. M. *Phys. Rev. B* **1994**, *49*, 755.
(23) Nymand, T. M.; Linse, P. *J. Chem. Phys.* **2000**, *112*, 6152.
(24) Lopez-Lemus, J; Alejandre, J. *Mol. Phys.* **2003**, *101*, 743.
(25) Bennett, C. H. *J. Comput. Phys.* **1976**, *22*, 245.
(26) Lu, N.; Singh, J. K.; Kofke, D. A. *J. Chem. Phys.* **2003**, *118*, 2977.
(27) Deitrick, G. L.; Scriven, L. E.; Davis, H. T. *J. Chem. Phys.* **1989**, *90*, 2370.
(28) Mcmullan, R. K.; Jeffrey, G. A. *J. Chem. Phys.* **1965**, *42*, 2725.
(29) Chialvo, A. A.; Bartók, A.; Baranyai, A. *J. Mol. Liq.* **2006**, *129*, 120.
(30) Harvey, A. H.; Sengers, J. M. H. L. *AIChE J.* **1990**, *36*, 539.
(31) Harvey, A. H. *AIChE J.* **1996**, *42*, 1491.
(32) NIST Chemistry WebBook. http://webbook.nist.gov/chemistry/ (2010).
(33) Docherty, H.; Galindo, A.; Vega, C.; Sanz, E. *J. Chem. Phys.* **2006**, *125*, 074510.
(34) Keisuke, M.; Ryo, O.; Sum, A. K.; Yasuoka, K. Gibbs Ensemble Monte Carlo Simulations for Methane, Liquid Water and Methane/Hydrate Phase Equilibrium. *Proceedings of the 6th International Conference of Gas Hydrates*; Vancouver, British Columbia, Canada, July 6−10, 2008.
(35) Jhaveri, J.; Robinson, D. B. *Can. J. Chem. Eng.* **1963**, *43*, 75.

(36) Deaton, W. M.; Frost, E. M. Gas hydrates and their relation to the operation of natural-gas pipe lines. *U.S. Bur. Mines Monograph* **1946**, *8*, 101.
(37) Marshall, D. R.; Saito, S.; Kobayashi, R. *AIChE J.* **1964**, *10*, 202.
(38) Sloan, E. D.; Fleyfel, F. *Fluid Phase Equilib.* **1992**, *96*, 223.
(39) Handa, Y. P. *J. Chem. Thermodyn.* **1986**, *18*, 891.
(40) Handa, Y. P. Calometric studies of laboratory synthesized and naturally occurring gas hydrates. AIChE Annual Meeting, Miami Beach, Nov 2−7, 1986.
(41) Munck, J.; Skjold-Jørgensen, S.; Rasmussen, P. *Chem. Eng. Sci.* **1988**, *43*, 2661.
(42) Sizov, V.; Piotrovskaya, E. M. *J. Phys. Chem. B* **2007**, *111*, 2886.
(43) Tanaka, H. *J. Chem. Phys.* **1994**, *101*, 10833.
(44) Ripmeester, J. A.; Ratcliffe, C. I. *J. Phys. Chem.* **1988**, *92*, 337.
(45) Sum, A. K.; Burruss, R. C.; Sloan, E. D. *J. Phys. Chem. B* **1997**, *101*, 7371.
(46) Galloway, T. J.; Ruska, W.; Chappelear, P. S.; Kobayashi, R. *Ind. Eng. Chem. Fundam.* **1970**, *9*, 237.
(47) de Roo, J. L.; Peters, C. J.; Lichtenthaler, R. N.; Diepen, G. A. M. *AIChE J.* **1983**, *29*, 651.
(48) Handa, Y. P. *J. Chem. Thermodyn.* **1986**, *18*, 915.
(49) Klauda, J. B.; Sandler, S. I. *J. Phys. Chem. B* **2002**, *106*, 5722.
(50) Sun, R.; Duan, Z. *Geochim. Cosmochim. Acta* **2005**, *69*, 4411.

JP911032Q